

# The Kinematic and Microphysical Control of Lightning Rate, Extent and NO<sub>x</sub> Production

Lawrence D. Carey<sup>1\*</sup>, William Koshak<sup>2</sup>, Harold Peterson<sup>3</sup>, Retha Matthee<sup>1</sup>, and A. Lamont Bain<sup>1</sup>

1. Department of Atmospheric Science, University of Alabama in Huntsville, Huntsville, Alabama, USA
2. Earth Science Office, NASA Marshall Space Flight Center, Huntsville, AL, USA
3. Universities Space Research Association (USRA), Huntsville, AL, USA

**ABSTRACT:** The purpose of this study is to investigate the kinematic and microphysical control of lightning properties, particularly those that may govern the production of nitrogen oxides via lightning (LNO<sub>x</sub>), such as flash rate, type and extent. The NASA Lightning Nitrogen Oxides Model (LNOM) is applied to lightning observations following ordinary convective cells through their lifecycle. LNOM provides estimates of flash rate, flash type, channel length distributions, lightning segment altitude distributions (SADs) and LNO<sub>x</sub> production profiles. For this study, LNOM is applied in a Lagrangian sense to multicell thunderstorms over Northern Alabama on 21 May 2012 during the Deep Convective Clouds and Chemistry (DC3) experiment. The LNOM lightning characteristics and LNO<sub>x</sub> production estimates are compared to the evolution of updraft and precipitation properties measured from a dual-Doppler and polarimetric radar network.

## INTRODUCTION

The Deep Convective Clouds and Chemistry (DC3) experiment seeks to quantify the relationships between storm physics, dynamics, lightning characteristics and the production of nitrogen oxides via lightning (LNO<sub>x</sub>). Ultimately, these relationships can be used to parameterize LNO<sub>x</sub> in numerical cloud models lacking explicit prediction of cloud electrical and lightning processes [e.g., Pickering et al. 1998; Barthe and Barth 2008; Barthe et al. 2010]. The specific focus of this study is to investigate the kinematic and microphysical control of lightning properties, particularly those that may govern LNO<sub>x</sub> production, such as flash rate, type (i.e., intracloud vs. cloud-to-ground) and extent across northern Alabama during DC3. Prior studies have demonstrated that lightning flash rate and type are correlated to kinematic and microphysical properties in the mixed-phase region of thunderstorms such as updraft volume and graupel mass.

More study is required to generalize these relationships in a wide variety of storm modes and meteorological conditions. Less is known about the co-evolving relationship between storm physics, morphology and three-dimensional flash extent, despite its obvious importance for LNO<sub>x</sub> production. To address this conceptual gap, the NASA Lightning Nitrogen Oxides Model (LNOM) is applied to North Alabama Lightning Mapping Array (NALMA) and Vaisala National Lightning Detection Network<sup>TM</sup>

---

\* Contact information: Lawrence D. Carey, Department of Atmospheric Science, University of Alabama in Huntsville, 320 Sparkman Drive, Huntsville, AL, USA, Email: [larry.carey@nsstc.uah.edu](mailto:larry.carey@nsstc.uah.edu)

(NLDN) observations following ordinary convective cells through their lifecycle. LNO<sub>x</sub> provides estimates of flash rate, flash type, channel length distributions, lightning segment altitude distributions (SADs) and lightning NO<sub>x</sub> production profiles. For this study, LNO<sub>x</sub> is applied in a Lagrangian sense to multicell thunderstorms over Northern Alabama on 21 May 2012 during DC3 in which aircraft observations of NO<sub>x</sub> are available for comparison. The LNO<sub>x</sub> lightning characteristics and LNO<sub>x</sub> production estimates are compared to the evolution of updraft and precipitation properties inferred from dual-Doppler and polarimetric radar analyses applied to observations from a nearby radar network.

## BACKGROUND

Based on numerous laboratory [e.g., Takahashi et al. 1978; Saunders 1994; Saunders and Peck 1998] and observational [Dye et al. 1986; 1989] studies, the primary means for particle charging in thunderstorms is thought to be a non-inductive mechanism, which involves rebounding collisions between graupel and small ice crystals in the presence of supercooled water. Particle fall speed differences and convective motions in a vigorous updraft result in storm scale charge separation, strong electric fields sufficient for breakdown and lightning. Because of its ability to identify and quantify graupel and convective updrafts, dual-polarization and multi-Doppler radar have been used to study the microphysical and kinematic control of lightning flash rate [e.g., Carey and Rutledge 1996; 2000; Wiens et al. 2005; Deierling et al. 2008; Deierling and Petersen 2008]. In these studies, graupel amount (e.g., graupel echo volume or precipitation ice mass) and updraft strength (e.g., maximum updraft, updraft volume) were shown to be highly correlated to the total (intracloud + cloud-to-ground) lightning flash rate.

Less has been documented regarding the kinematic and microphysical control of flash extent. Bruning and MacGorman [2013] presented data from supercells that support their theoretical prediction from electrostatics that frequent breakdown and large flash extents are opposed. In Bruning and MacGorman [2013] and prior studies [e.g., Carey et al. 2005; Kuhlman et al. 2009; Weiss et al. 2012], high flash rates characterized by small extents were located near the updraft region while large flashes tended to occur infrequently away from the convective generator and within the stratiform precipitation or anvil region of mesoscale convective systems and supercells, respectively. The correspondence between kinematic and electrical energy spectra in Bruning and MacGorman [2013] suggests that advection of charge-bearing precipitation by the storm's flow, including in turbulent eddies, couples the kinematic and electrical properties of a thunderstorm, including presumably lightning flash extent.

LNO<sub>x</sub> production is thought to be controlled by lightning flash rate, type, extent, and other properties [e.g., Pickering et al. 1998; Wang et al. 1998; Barthe and Barth 2008; Cooray et al. 2009; Barthe et al. 2010; Peterson et al. 2010; Koshak et al. 2014]. In several modeling studies, LNO<sub>x</sub> production is based primarily on the total flash rate [e.g., Pickering et al. 1998; Barthe and Barth 2008]. In laboratory studies of simulated lightning, Wang et al. [1998] find that flash extent, multiplicity and peak current may also be important. There is currently some disagreement in the literature as to whether the lightning type (e.g. cloud-to-ground or intracloud) has any effect on the amount of LNO<sub>x</sub> generated per flash. Some modeling studies suggest that there is roughly an order of magnitude difference in LNO<sub>x</sub> production between cloud-to-ground and intracloud lightning [Price et al. 1997; Pickering et al. 1998; Koshak et al. 2014]. Price et al. [1997] state that cloud-to-ground flashes produce more LNO<sub>x</sub> than intracloud flashes

based on the stronger energetics associated with cloud-to-ground flashes. Pickering et al. [1998] found that simulated cloud-to-ground flashes produced larger instantaneous  $\text{LNO}_x$  values versus intracloud flashes. In a modeling study that utilizes three-dimensional lightning mapping array observations as input, Koshak et al. [2014] find roughly an order of magnitude greater  $\text{LNO}_x$  produced per cloud-to-ground flash than per intracloud flash. On the other hand, the observational studies of DeCaria et al. [2000, 2005], Fehr et al. [2004], Ridley et al. [2005] and Ott et al. [2007] suggest that cloud-to-ground and intracloud flashes may produce approximately the same amount of  $\text{LNO}_x$  per flash. In a field study by Dye et al. [2000], it was determined that intracloud flashes were the more significant contributor to  $\text{LNO}_x$  in an isolated Colorado supercell with high intracloud to cloud-to-ground ratio. Barthe and Barth [2008] performed sensitivity studies, which showed that varying the intracloud to cloud-to-ground ratio yielded very little difference in the  $\text{LNO}_x$  profile within their modeling study.

## DATA AND METHODOLOGY

In order to explore the co-evolving relationship between storm kinematics, microphysics, lightning properties and  $\text{LNO}_x$  production in ordinary convection, the NASA LNOM [Koshak et al. 2014] is applied to NALMA and NLDN lightning observations and compared to multi-Doppler and polarimetric radar observations of a multicell cluster on 21 May 2012 over northern Alabama taken during the DC3 field experiment [Bain 2013; Bain et al. 2013; Carey et al. 2014].

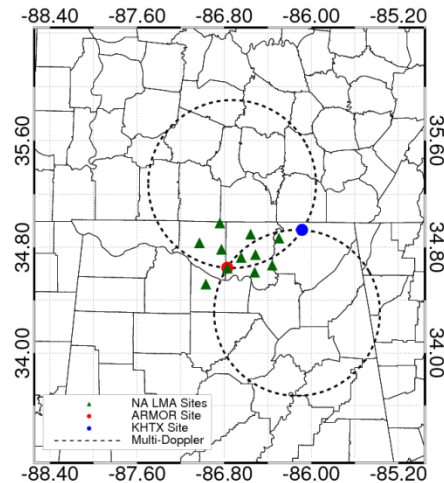


**Fig. 1.** A map of the DC3 Alabama domain. The green triangles represent NA LMA VHF antennas. The solid red dot represents the location of the ARMOR radar. The solid blue dot represents the location of KHTX. The short-dashed lines represent regions where multi-Doppler wind synthesis can be performed.

### *DC3 radar and lightning observations*

DC3 took place in May – June 2012 over Northern Alabama and two other locations (Colorado and Oklahoma/Texas) [Barth et al. 2013]. For DC3 Alabama, the Advanced Radar for Meteorological and Operational Research (ARMOR) [Petersen et al. 2005] and the Weather Surveillance Radar - 1988 Doppler (WSR-88D) comprises the dual-Doppler and dual-polarization radar network (Fig. 1). The

S-band WSR-88D is operated and owned by the National Weather Service (NWS) and is located at Hytop, AL (KHTX). The C-band ARMOR radar is located at the Huntsville International Airport and is co-owned by the University of Alabama in Huntsville (UAH) and WHNT. ARMOR and KHTX have a beamwidth of  $1^\circ$  and  $.92^\circ$ , respectively, and both operate in a simultaneous transmit and receive of both the horizontal and vertical channels. ARMOR and KHTX are both capable of measuring horizontal reflectivity ( $Z_h$ ), Doppler velocity ( $V_r$ ), differential reflectivity ( $Z_{dr}$ ), the co-polar correlation coefficient ( $\rho_{hv}$ ) and differential phase ( $\Phi_{dp}$ ). The specific differential phase ( $K_{dp}$ ) for ARMOR is computed using a method that is outlined in Bringi and Chandrasekar [2001]. Additional specifications of ARMOR are discussed in Petersen et al. [2005]. The relatively close proximity of ARMOR and KHTX (approximately 70 km) presents the opportunity for three dimensional wind retrievals within the highlighted areas denoted in Fig. 1.

The NALMA [Goodman et al. 2005] is located within the dual-Doppler network (Fig. 1). NALMA is owned and operated by the National Aeronautics and Space Administration-Marshall Space Flight Center (NASA MSFC). The network consists of 11 very high frequency (VHF) antennas across northern AL that detect radiation emissions from propagating leaders associated with lightning using a time-of-arrival technique [Koshak et al. 2004; Goodman et al. 2005]. The NALMA in conjunction with the NLDN allow for a detailed depiction of total lightning. The multicell cluster analyzed on 21 May 2012 occurred within the dual-Doppler radar domain shown in Fig. 1 and was always within 100 km of the center of the NALMA VHF network (Fig. 2), allowing a complete depiction of kinematic, microphysical and lightning properties.

### ***Radar methodology***

Both ARMOR and KHTX radar data underwent a vigorous quality control process implemented at UAH. As a result of ARMOR's relatively shorter wave length (relative to KHTX), propagation effects occur with the presence of heavy rain. To address this issue, all raw ARMOR data were corrected for attenuation and differential attenuation using a self-consistency method outlined in Bringi et al. [2001]. The corrected ARMOR and raw KHTX radar data were then manually inspected using the National Center for Atmospheric Research's (NCAR) SOLO radar visualization and editing software. During this labor-intensive process, aliased Doppler velocities were corrected and spurious echoes associated with second trip echoes, ground targets and anomalous propagation were removed. In the event that ARMOR operations consisted of sector volumes, an internal method for correcting any azimuth pointing angle error was employed.

Radiosonde observations (RAOBs) from the UAH mobile ballooning facility were quality controlled by specialists at NCAR using the techniques outlined in Loehrer et al. [1996]. The combination of temperature data and the polarimetric radar variables from ARMOR allowed for the use of a fuzzy logic based particle identification algorithm, hereafter NCAR PID [Vivekanandan et al. 1999; Straka et al. 2000]. While originally developed for use at S-Band, modifications to the NCAR PID [Deierling et al. 2008] were necessary owing to both ARMOR's C-band wavelength and operational mode (simultaneous transmit of H and V results in the inability to attain the linear depolarization ratio [LDR]). With information from NCAR PID, several microphysical quantities thought to be relevant for the NIC mechanism (e.g., graupel echo volume, graupel mass) can be computed.

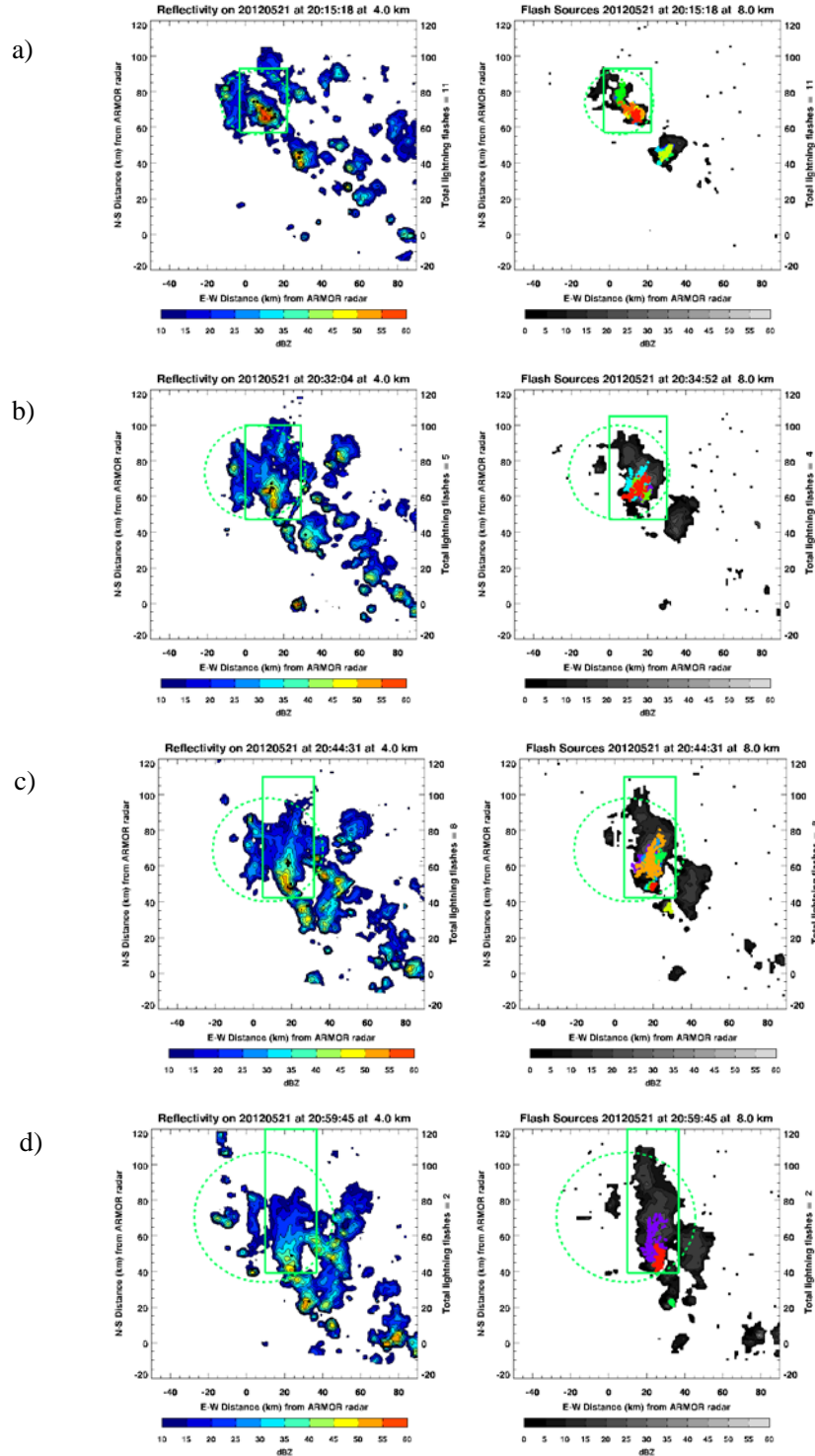


**Fig. 2.** Summary depiction of the evolution of the ARMOR radar and NALMA lightning structure in a multicell storm cluster on 21 May 2012. *Left:* Radar reflectivity (dBZ, color shaded) at 4 km and NALMA flash origins (dots) and *Right:* Radar reflectivity (dBZ grey shade) at 8 km and NALMA VHF sources associated with individual flashes (color coded by flash) at a) 2015, b) 2032, c) 2045, and d) 2100 UTC. The solid green box and the dashed circle depict the radar analysis domain and LNUM analysis cylinder, respectively.

Once the quality control of ARMOR and KHTX data was completed, both sets of data were gridded using NCAR's REORDER package [Mohr et al. 1986]. Polarimetric and Doppler radar quantities (excluding NCAR PID data) were gridded from radar space to a Cartesian grid with spacing of 1 km in x, y and z using the Cressman Weighting scheme [Cressman 1959] and radii of influence of 1 km in the horizontal and vertical. The NCAR PID information was also gridded to Cartesian space with 1 km grid spacing in the horizontal and vertical dimensions using a Nearest Neighbor Weighting scheme and similar radii of influence. For this study, graupel volume and graupel mass were computed. Consideration was only given to the mixed phase region between the -10 °C and -40 °C layer (roughly 6 km to 10 km AGL). This so-called "charging region", as termed by Latham et al. [2004], is theorized to be the region in which active NIC of graupel primarily occurs. The number of grid boxes associated with graupel particles identified by the NCAR PID were summed over the height layer corresponding to the -10 °C and -40 °C temperature layer and then multiplied by the grid box volume to attain the desired graupel echo volume. For grid boxes identified as containing graupel by the NCAR PID in the same height layer, an estimate of graupel mass was obtained from a reflectivity – ice mass (Z-M) relationship found in Carey and Rutledge [2000], which is based on the Rayleigh scattering approximation for an assumed exponential ice particle size distribution. The non-precipitation ice mass in the anvil region aloft was calculated using the Z-M relation from Heymsfield and Palmer [1986] for all  $Z_h > 0$  dBZ at temperature (T) < -40°C.

After both ARMOR and KHTX radar data are gridded to a common Cartesian plane, NCAR's Custom Editing and Display of Reduced Cartesian Space (CEDRIC) tool was used for the multi-Doppler wind synthesis [Miller and Frederick 1998]. A variational integration method of the mass continuity equation was invoked due to the expected minimization of divergence errors at the upper boundary condition when determining vertical motion from estimates of the U and V components of the horizontal wind as well as estimates of particle fall speed. The vertical motion field is then utilized to compute the convective (> 5 m s<sup>-1</sup>) updraft volume in the -10 °C and -40 °C temperature layer. Additional details on the radar data and methodology can be found in Bain [2013].

### ***NASA Lightning Nitrogen Oxides Model***

The NASA LNO<sub>x</sub> Model [Koshak et al. 2014] ingests lightning VHF source location and time-of-occurrence data such as obtained from the NALMA. It also ingests location, time-of-occurrence, peak current, and stroke multiplicity data from the NLDN. These data are used to determine the flash type (cloud-to-ground or intracloud) of each flash occurring within the LNO<sub>x</sub> analysis cylinder (height 0–20 km and variable radius). A Lagrangian (i.e., storm following) analysis cylinder of variable radius was subjectively drawn around the storm cluster of interest centered at each radar volume time (Fig. 2) in order to compare the evolution of LNO<sub>x</sub> output properties to the radar observations. The LNO<sub>x</sub> analyzes the VHF sources to estimate the total channel length of each flash. Both ground and cloud flashes are analyzed. LNO<sub>x</sub> chops each portion of a flash contained in the analysis cylinder into 10-m segments and sums these segments in each 100-m layer to determine the Segment Altitude Distribution (SAD) within the cylinder. SAD's at all heights are added to estimate flash extent. Finally, LNO<sub>x</sub> computes the vertical LNO<sub>x</sub> production profile from observed lightning properties in the cylinder using model parameterizations based on laboratory [Wang et al. 1998; Peterson et al. 2010] and theoretical [Cooray et al. 2009] studies. Details on the LNO<sub>x</sub> production parameterization can be found in Koshak et al. [2014].

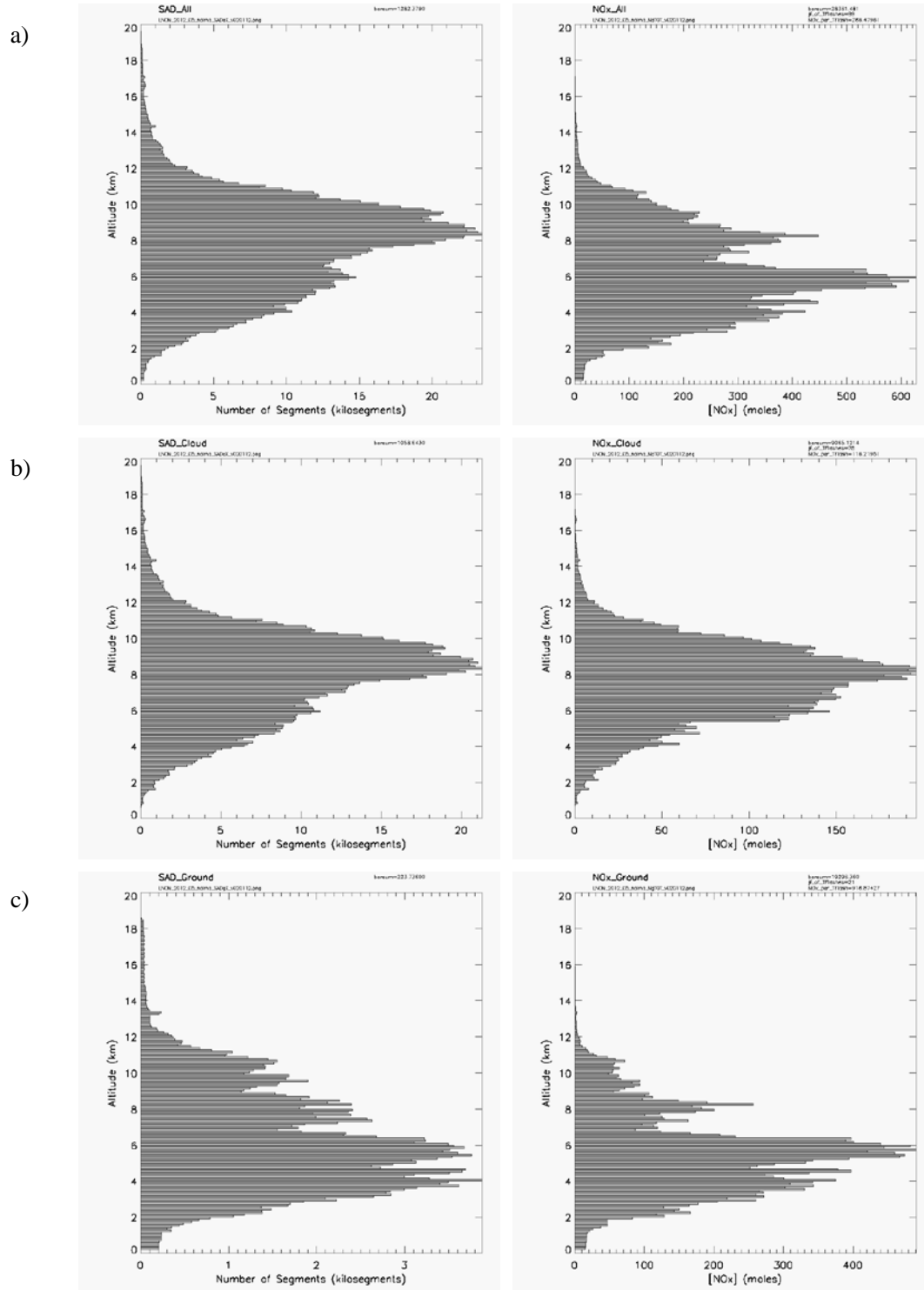


**Fig. 3.** Storm integrated vertical profiles of lightning extent and LNO<sub>x</sub> production inferred from the LNO<sub>m</sub> following a multicell storm cluster on 21 May 2012 from 1953 to 2104 UTC. *Left:* SAD profiles (kilosegments) and *Right:* LNO<sub>x</sub> production profiles (moles) for a) all lightning (cloud-to-ground and intracloud combined), b) intracloud lightning only and c) cloud-to-ground lightning only.

## RESULTS

For this study, the evolution of a multicell convective cluster observed in Northern Alabama (Fig. 1) on 21 May 2012 was analyzed from 1953 to 2104 UTC using radar and lightning observations (Fig.2) and the NASA LNO<sub>x</sub>. Although beyond the scope of the current analysis, aircraft observations taken in and around this multicell thunderstorm during the DC3 field campaign should eventually allow the comparison of in situ observed NO<sub>x</sub> and LNO<sub>x</sub> derived LNO<sub>x</sub> production profiles.

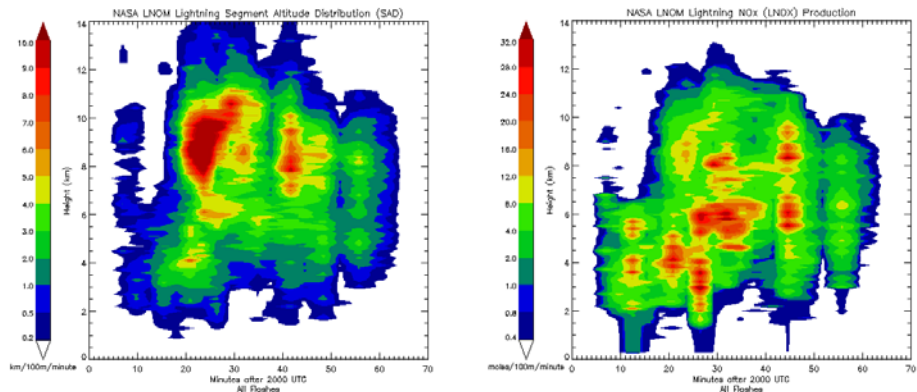
Storm integrated summary profiles of LNO<sub>x</sub> SAD and LNO<sub>x</sub> production during the roughly one hour period on 21 May 2012 are first presented followed by time-height cross sections of storm integrated SAD and LNO<sub>x</sub> production. Time-height cross-sections of maximum reflectivity, graupel echo volume, graupel mass and convective ( $> 5 \text{ m s}^{-1}$ ) updraft volume in the charging zone are then presented for comparison with the LNO<sub>x</sub> profile properties. The time series of storm integrated LNO<sub>x</sub> SAD and LNO<sub>x</sub> production profiles are then carefully compared to the time-series evolution of radar-inferred graupel echo volume, convective updraft volume, and graupel mass in the mixed phase zone. LNO<sub>x</sub> flash extent is also related to the non-precipitation ice mass in the anvil region. In each case, the Pearson correlation coefficient between the time series of radar and LNO<sub>x</sub> properties are computed to quantify the potential kinematic and microphysical control of flash rate, flash extent and LNO<sub>x</sub> production.

### *LNO<sub>x</sub> SAD and LNO<sub>x</sub> production*

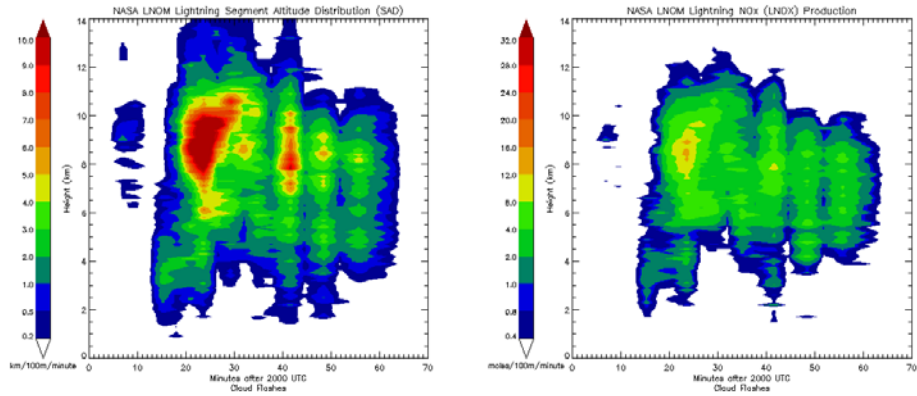
In order to characterize the vertical structure of lightning extent and associated production of nitrogen oxides during the one hour period of the multicell cluster, profiles of storm integrated LNO<sub>x</sub> SAD (left column) and LNO<sub>x</sub> production (right column) are presented in Fig. 3. For all (i.e., ground + cloud) lightning flashes, there is a peak in SAD between 8 and 10 km altitude with a secondary peak or shelf in SAD at about 6 km (Fig. 3a). The cloud flash SAD is very similar with a dominant peak at 8 to 10 km and less pronounced shelf at 6 km (Fig. 3b). In fact, the cloud flash SAD appears to comprise a significant fraction of the all flash SAD. The ground flash SAD is significantly smaller, somewhat multi-modal with several relative maxima in the vertical and dominant peaks between 4 and 6 km altitude (Fig. 3c). As expected, there are more 10-m lightning segments at low levels in cloud-to-ground flashes in a relative sense than in intracloud flashes. In an absolute sense, intracloud lightning tends to dominate the SAD at nearly all levels except at the lowest levels (e.g.,  $< 3 \text{ km}$ ) where ground and cloud flash extents are comparable.

The LNO<sub>x</sub> production in all flashes is multimodal with a dominant peak at 6 km and secondary peaks around 4 km and 8 km altitudes (Fig. 3a). The LNO<sub>x</sub> production of intracloud flashes has a clear peak at 8 km with a broader maximum between 6 and 10 km, beyond which the SAD drops rapidly in both directions (Fig. 3b). Despite dominating the SAD, the peak intracloud LNO<sub>x</sub> production peak at 8 km is less than the corresponding cloud-to-ground LNO<sub>x</sub> production peak at 6 km (Fig. 3c). The ground LNO<sub>x</sub> production profile also has secondary peaks at 8 km and roughly 4 km. The ground LNO<sub>x</sub> production is generally larger than the cloud LNO<sub>x</sub> production at altitudes  $\leq 6.5 \text{ km}$ . At altitudes  $> 6.5 \text{ km}$ , the LNO<sub>x</sub> production for cloud and ground flashes are more comparable.

a)



b)



c)

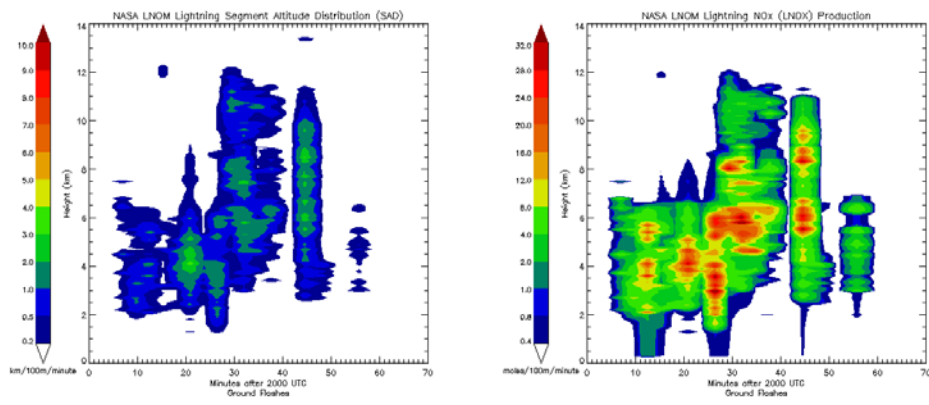


**Fig. 4.** Time-height cross-sections of *Left:* LNM SAD (km / 100m / minute) and *Right:* LNM LNO<sub>x</sub> production (moles / 100 m / minute) for a) all flashes (cloud-to-ground and intracloud combined), b) intracloud flashes only, and c) cloud-to-ground flashes only. Time is in minutes after 2000 UTC.

Time-height cross-sections of LNOM SAD (left column) are provided in Fig. 4 for total lightning (Fig. 4a), intracloud lightning (Fig. 4b) and cloud-to-ground lightning (Fig. 4c). Both intracloud and cloud-to-ground lightning flashes begin around 2007 UTC. Total and intracloud lightning SAD rapidly increases by 2015 UTC, reaching a maximum around 2024 UTC, especially aloft in the charging region between 6 km and 10 km. The total and intracloud lightning SAD decrease somewhat between 2024 and 2037 UTC and then increases again to a relative maximum at 2042 UTC, especially in the charging zone. The total and intracloud lightning SAD decrease again after 2049 UTC until they reach a final relative maximum at about 2056 UTC. After 2056 UTC, the total and intracloud lightning SAD decrease as the storm cluster weakens and lightning activity ceases by 2104 UTC. As noted above, the intracloud flash SAD dominates the total lightning flash SAD as Figs. 4a and 4b are very similar in appearance especially at altitudes above 6 km. At lower levels the ground SAD (Fig. 4c) contributes more significantly to the total lightning SAD (Fig. 4a). SAD associated with ground flashes is more uniformly continuous during the roughly 1 hour lifecycle of this storm cluster. One notable trend in the cloud-to-ground activity is the increase in ground SAD in the charging zone aloft at altitudes  $> 6$  km after the peak in total and intracloud lightning SAD at 2024 UTC. VHF sources associated with these flashes typically start at  $> 6$  km altitude yet have an associated NLDN detected ground flash location. Although these flashes are categorized as ground flashes by the LNOM and are treated as such in this study, they are often categorized as IC-CG hybrid flashes [e.g., Matthee and Carey 2014]. In this multicell storm cluster, such ground flashes with initial VHF source and extensive SAD  $> 6$  km have the largest flash extent on average of all flash types [Matthee and Carey 2014].

Time-height cross-sections of  $\text{LNO}_x$  production (right column) are provided in Fig. 4 for total lightning (Fig. 4a), intracloud lightning (Fig. 4b) and cloud-to-ground lightning (Fig. 4c). Unlike SAD, total  $\text{LNO}_x$  production is a more equal combination of cloud and ground  $\text{LNO}_x$  production at heights above 6 km. At 6 km and below, the ground  $\text{LNO}_x$  production dominates the total lightning  $\text{LNO}_x$  production. The column integrated ground  $\text{LNO}_x$  production dominates the column integrated total  $\text{LNO}_x$  production with both quantities peaking broadly between 2021 UTC and 2038 UTC (overall peak at 2027 UTC) and again more sharply at 2045 UTC. Similar to the cloud SAD, the cloud  $\text{LNO}_x$  production peaks at 2024 UTC with secondary maxima at 2042, 2049 and 2056 UTC.

### ***Radar kinematic and microphysical properties***

Time-height cross-sections of maximum reflectivity (Fig. 5a), graupel volume (Fig. 5b), graupel mass (Fig. 5c), and updraft volume (Fig. 5d) are provided for comparison with the LNOM SAD and  $\text{LNO}_x$  production. The first radar inferred pulse in the updraft volume, maximum reflectivity and graupel echo volume and mass from 2001 to 2012 UTC is associated with the first SAD and  $\text{LNO}_x$  production. A continued surge in the updraft up to its peak at 2021 UTC results in rapid coincident increases and maxima in the graupel echo volume and graupel mass. Likely associated with an explosion in the occurrence of graupel-ice collisions and charging, the total and intracloud lightning SAD also rapidly increase and peak at 2024 UTC. The intracloud  $\text{LNO}_x$  production also peaks at 2024 UTC. However, the ground and total  $\text{LNO}_x$  production both experience broad maxima between 2021 and 2038 UTC during which time the updraft volume, graupel volume and graupel mass are generally decreasing in the charging zone. Secondary maxima in updraft volume, graupel volume and mass after 2040 UTC are associated with secondary maxima in the SAD and  $\text{LNO}_x$  production.

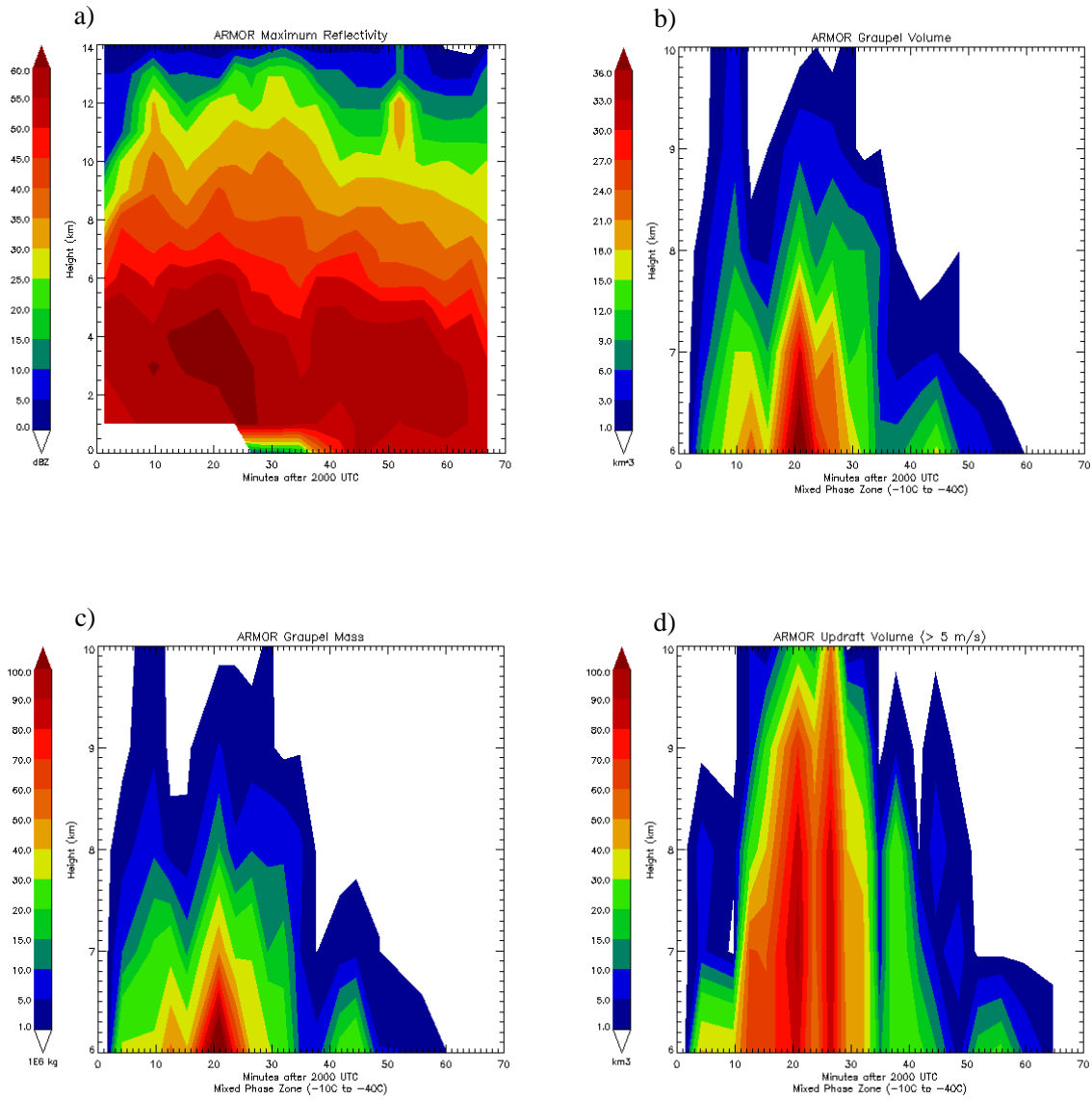


**Fig. 5.** Time-height cross-sections of radar microphysical and kinematic quantities associated with the multicell cluster on 21 May 2012. a) maximum reflectivity (dBZ, color shaded as shown), b) graupel echo volume in the charging region ( $\text{km}^3$ , color shaded as shown), c) graupel mass in the charging region ( $1 \times 10^6$  kg, color shaded as shown), and updraft volume  $> 5 \text{ m s}^{-1}$  ( $\text{km}^3$ , color shaded as shown). Time is in minutes after 2000 UTC. Maximum reflectivity is shown for all heights while graupel volume, graupel mass and updraft volume are only shown in the charging zone ( $-10^\circ\text{C} < T < -40^\circ\text{C}$ ) or from 6 to 10 km.

### *Time series of LNO<sub>x</sub> lightning properties*

Cloud flashes make up the over-whelming number of total lightning flashes as shown in the time series of flash count in Fig. 6. Both cloud and total lightning activity begins around 2007 UTC and rapidly increases to a maximum around 2024 UTC. After 2024 UTC, the cloud and total lightning flash activity decreases to a relative minimum around 2035-2038 UTC. Another relative maximum in cloud and total lightning flash count occurs at 2045 UTC. As also shown in Fig. 6, the ground flash count has no predominant peak (actual peak occurred at 2013 UTC) but maintains a fairly steady flash count through most of the cluster lifecycle.

The average LNO<sub>x</sub> flash extent (Fig. 7) increases during the ramp up in the flash count (Fig. 6) associated with convective generator. However, the average flash extent lags the flash count and both properties are somewhat anti-correlated (cf., Figs. 6 and 7). The largest average flash extents tend to occur after the maximum flash count associated with the convective generator. Late in the storm lifecycle, relative maxima in flash count tend to be associated with relative minima in the flash extent (e.g., see 2045 UTC) and vice versa (e.g., see 2052 UTC).

The total flash extent (i.e., the sum of lightning extent for all flashes during a given time period) is provided in Fig. 8. The total flash extent for all flashes (i.e., cloud and ground) is dominated largely by the total flash extent of cloud flashes, which is due to the much larger cloud flash counts (Fig. 6) and somewhat similar average flash sizes (Fig. 7). The average cloud flash extent is 135.7 km while the average ground flash extent is 106.5 km. Meanwhile, the intracloud to cloud-to-ground ratio (IC:CG) is 3.7. Overall, the total extent of lightning flashes is largely controlled by flash rate and not so much by average flash size (cf., Figs. 6, 7 and 8). In fact, the Pearson correlation coefficient between total flash extent and flash rate is 0.9 for all flashes.

The LNO<sub>x</sub> production is shown in Fig. 9. The cloud LNO<sub>x</sub> production is highly correlated to the total cloud flash extent (Fig. 8), which appears to be largely controlled by flash rate as noted above. More specifically, the Pearson correlation coefficient between cloud LNO<sub>x</sub> production and total cloud flash extent is 0.99. Thus, total cloud flash extent explains nearly all the variation of the cloud LNO<sub>x</sub> production, which is a result of the LNO<sub>x</sub> production parameterization scheme in Koshak et al. [2014]. Similarly, the Pearson correlation coefficient between ground LNO<sub>x</sub> production and total ground flash extent is 0.95. As noted in Koshak et al. [2014], ground LNO<sub>x</sub> production is governed in part by other ground flash parameters (e.g., peak current) in LNO<sub>x</sub>. Despite the fact that total cloud flash extent is much larger than total ground flash extent (Fig. 8), the majority of LNO<sub>x</sub> production is still from ground flashes (Fig. 9). In other words, LNO<sub>x</sub> produces significantly more LNO<sub>x</sub> on average for ground flashes (919 moles/flash) than for cloud flashes (116 moles/flash) in this storm cluster. It is interesting to note that the LNO<sub>x</sub> production per ground flash is larger from 2026 UTC to 2045 UTC (Figs. 6 and 9) when the average ground flash extent is larger (Fig. 7). As noted earlier, many of these more extensive ground flashes are actually the hybrid intracloud-cloud-to-ground (IC-CG) flashes noted in Matthee and Carey [2014]. This period also accounts for some of the largest ground and hence total flash LNO<sub>x</sub> production for the storm cluster. From these results, we can conclude that the spatial extent of individual ground flashes can have a significant impact on the total LNO<sub>x</sub> production in a multicell storm cluster.

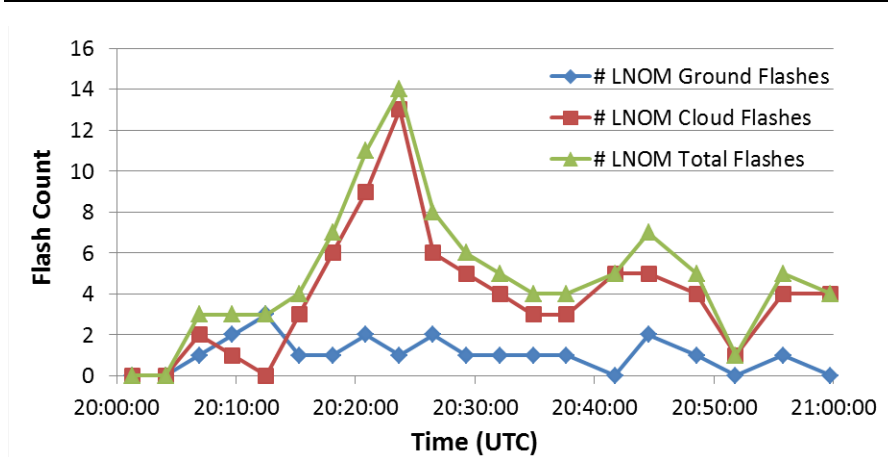


Fig. 6. Time series of LNOM lightning flash count for ground, cloud and all flashes.

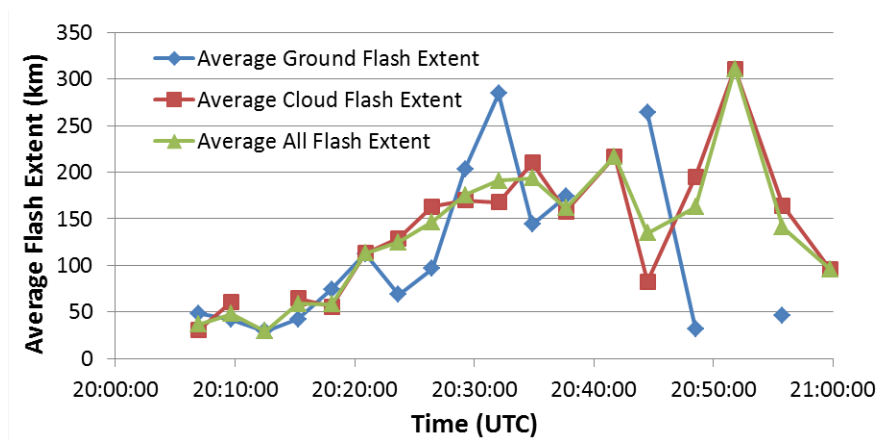


Fig. 7. Time series of LNOM average lightning flash extent (km) for ground, cloud and all flashes.

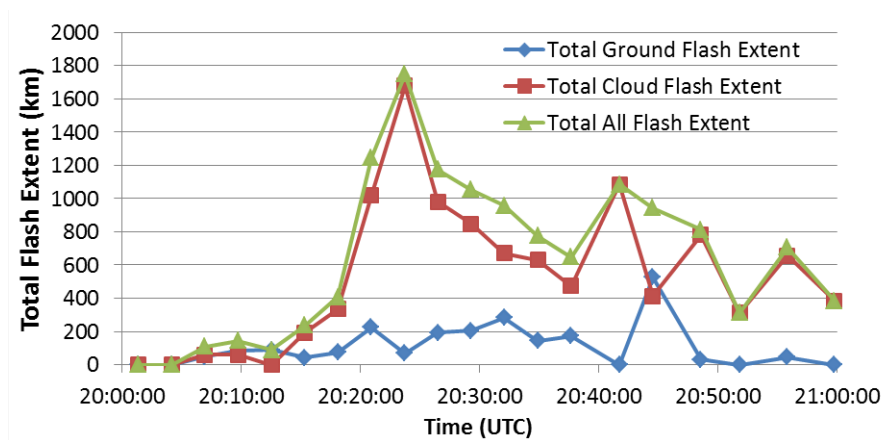


Fig. 8. Time series of LNOM total flash extent (km) for ground, cloud and all flashes.

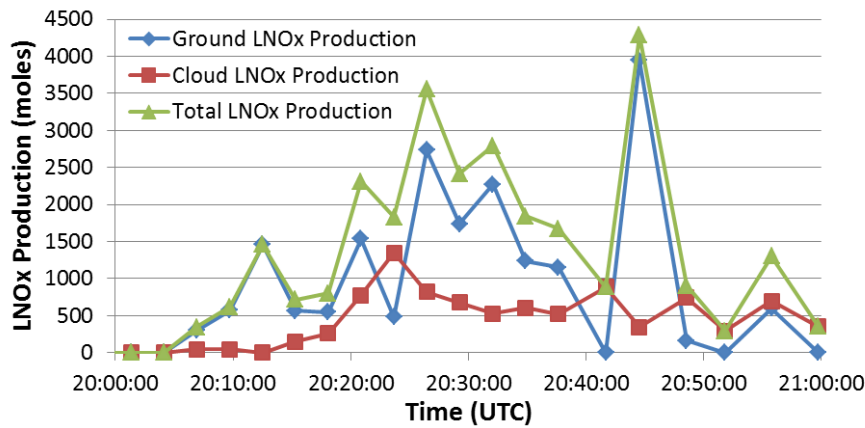


Fig. 9. Time series of LNOx production (moles) for ground, cloud and all flashes.

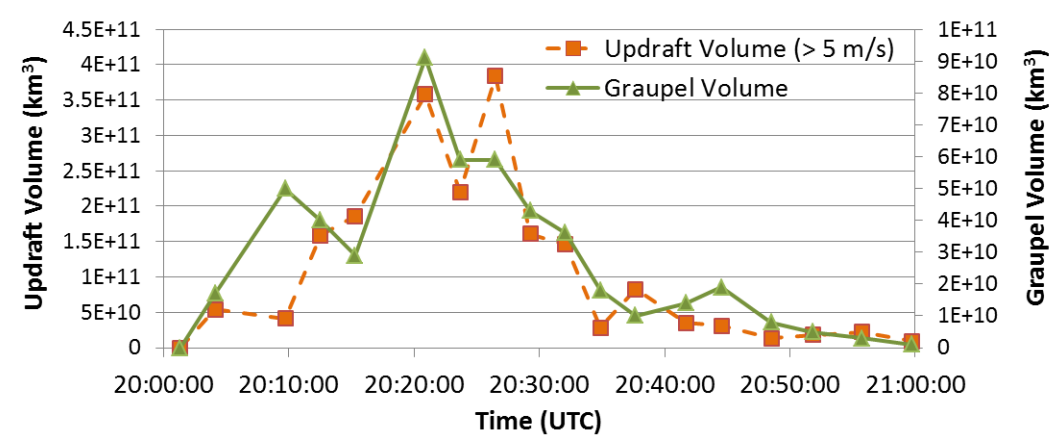


Fig. 10. Time series of radar updraft volume (km³) and graupel volume (km³) in the charging zone.

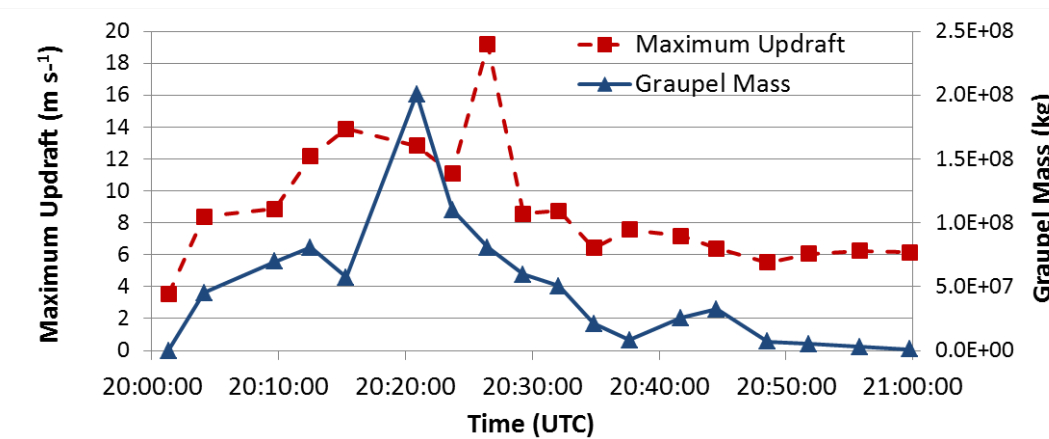
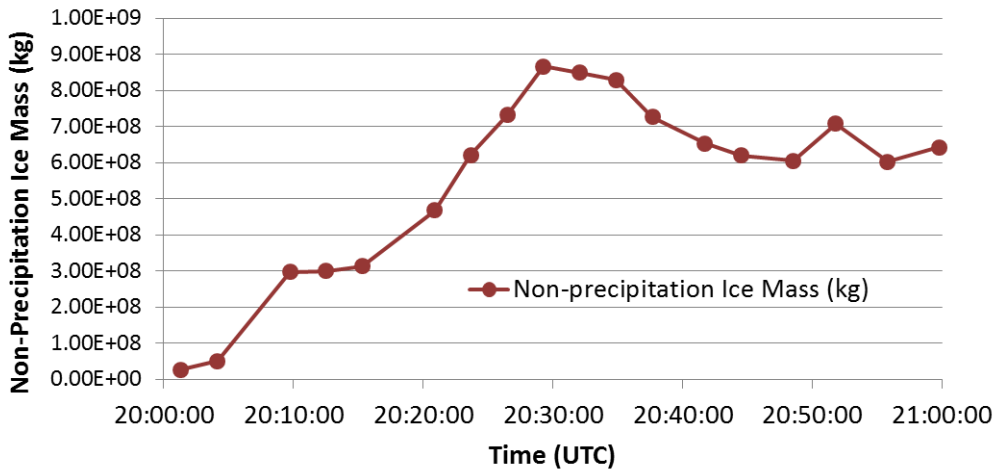


Fig. 11. Time series of radar maximum updraft (m s⁻¹) and graupel mass (kg) in the charging zone.



**Fig. 12.** Time series of radar non-precipitation ice mass (kg) for  $Z_h > 0$  dBZ at  $T < -40^\circ\text{C}$ .

### *Comparison of LNOM and radar time series*

The time series of radar inferred kinematic and microphysical properties that are associated with the convective generator are provided in Fig. 10 (updraft volume and graupel echo volume) and Fig. 11 (maximum updraft and graupel mass). By comparing Figs. 10 and 11 to Fig. 6, it is apparent that the flash rate increases along with the convective updraft and production of graupel in the charging zone, as has been seen in past studies. Rapid electrification and first lightning does not occur until after the maximum updraft in the charging zone exceeds  $8 \text{ m s}^{-1}$  [e.g., Zipser and Lutz 1994]. The graupel volume, graupel mass, updraft volume, and to a lesser extent, the maximum updraft are all reasonably well correlated to the total flash rate (Table 1) [e.g., Carey and Rutledge 1996; 2000; Wiens et al. 2005; Deierling et al. 2008; Deierling and Petersen 2008].

The radar parameters in Figs. 10 and 11 are not as well correlated (Table 1) with the total flash extent rate ( $\text{km min}^{-1}$ ), which is the total flash extent of all flashes (km) (Fig. 8) for a given radar sample period divided by the time period (min), or the total  $\text{LNO}_x$  production (mole) (Fig. 9). In fact, a comparison between Figs. 9, 10 and 11 reveals that the  $\text{LNO}_x$  production lags the graupel volume, graupel mass, updraft volume and maximum updraft. The correlations between these radar parameters and the  $\text{LNO}_x$  production increase when the radar parameters are shifted forward in time by 2 radar volumes (about 7 minutes on average) in order to account for the lag of the  $\text{LNO}_x$  production relative to the radar parameters.

As long as the convective generator is still active, the flash extent may be better correlated to thunderstorm ice anvil properties than to convective updraft or graupel. More specifically, it is hypothesized that the average all lightning (i.e., both cloud and ground combined) flash extent in Fig. 7 is physically related to the amount of non-precipitation ice mass (kg) in the anvil region of the storm cluster (Fig. 12). Comparing Figs. 7 and 12, it can be noted that the correlation between non-precipitation ice mass and the average extent of all flashes is strong ( $\rho = 0.82$ ), suggesting that the amount of non-precipitation anvil ice, which is likely carrying ample charge, controls the average extent of lightning

flashes in ordinary multicell convection. As long as the convective updraft is active and aiding in the collision, charging and storm scale separation of graupel and small ice particles, it is anticipated that non-precipitation ice mass aloft and flash extent will be well correlated.

**Table 1.** Pearson correlation coefficient ( $\rho$ ) between the time series of radar-inferred kinematic and microphysical quantities and LNO<sub>x</sub> total (cloud + ground) lightning properties for the multicell storm cluster on 21 May 2012. The values in parentheses in the LNO<sub>x</sub> production column are associated with a 2-lag correlation (i.e., the radar parameters are shifted forward in time by 2 radar volumes).

<b>Radar Parameter</b>	<b>Total Flash Rate (min<sup>-1</sup>)</b>	<b>Total Flash Extent Rate (km min<sup>-1</sup>)</b>	<b>Total LNO<sub>x</sub> Production (moles)</b>
Graupel Echo Volume (km <sup>3</sup> )	0.79	0.61	0.51 (0.66)
Graupel Mass (kg)	0.77	0.55	0.41 (0.63)
Updraft Volume (km <sup>3</sup> )	0.76	0.61	0.57 (0.72)
Maximum Updraft (m s <sup>-1</sup> )	0.60	0.41	0.50 (0.67)

## SUMMARY

In order to explore the co-evolving relationship between storm kinematics, microphysics, lightning properties and LNO<sub>x</sub> production in ordinary convection, the NASA LNOM was applied to NALMA and NLDN lightning observations and compared to multi-Doppler and polarimetric radar observations of a multicell thunderstorm on 21 May 2012 (1953 – 2104 UTC) over northern Alabama during DC3. The key findings of the study are summarized as follows:

1. The total (i.e., ground and cloud) and cloud flash segment altitude distributions are very similar with a dominant peak at 8 to 10 km and less pronounced shelf at 6 km. The cloud flash SAD comprises a significant fraction of the all flash SAD. The ground flash SAD is significantly smaller, somewhat multi-modal with a dominant peak between 4 and 6 km altitude. In an absolute sense, the cloud SAD dominates at all vertical levels except below 3 km.

2. Despite dominating the SAD, the cloud flash LNO<sub>x</sub> production peak at 8 km is less than the corresponding ground flash LNO<sub>x</sub> production peak at 6 km. The ground LNO<sub>x</sub> production is generally larger than the cloud LNO<sub>x</sub> production at all altitudes less than 6.5 km while above that height the two production terms are comparable.

3. One notable trend in the ground flash activity is the increase in ground SAD in the charging zone aloft at altitudes > 6 km *after* the simultaneous peaks in the total and cloud lightning flash rate, graupel volume/mass and convective updraft volume at 2024 UTC, which are all associated with convective generator. A large number of the LNOM ground flashes (i.e., associated with NLDN ground flash) during this time when the convective generator is weakening are categorized as IC-CG hybrid flashes because the VHF sources start at > 6 km altitude and have large extents aloft before coming to ground.

4. At heights below 6 km, the ground LNO<sub>x</sub> production dominates the column integrated lightning LNO<sub>x</sub> production associated with all flashes. Unlike SAD, total LNO<sub>x</sub> production is a more equal contribution of both cloud and ground LNO<sub>x</sub> production terms at heights above 6 km. Overall, column integrated ground LNO<sub>x</sub> production dominates the column integrated total LNO<sub>x</sub> production associated with all flashes with both quantities peaking *after* the simultaneous peaks in the convective updraft volume, graupel volume and flash rate.

5. The first radar inferred pulse in the updraft volume, maximum updraft, maximum reflectivity, and graupel volume/mass precede the first lightning flash and associated LNO<sub>x</sub> production. First lightning does not occur until the maximum updraft in the charging zone exceeds 8 m s<sup>-1</sup>. Graupel volume/mass, updraft volume and to a lesser extent maximum updraft are all reasonably well correlated to the total flash rate ( $\rho \approx 0.8$  except for maximum updraft where  $\rho \approx 0.6$ ).

6. The ground and total LNO<sub>x</sub> production both experience broad maxima after the peak in the convective generator when the updraft volume, graupel volume/mass are generally decreasing in the charging zone. These radar kinematic and microphysical parameters associated with the convective generator are not as well correlated to the total flash extent or the total LNO<sub>x</sub> production as they are to flash rates ( $\rho \approx 0.4$  to 0.6). The correlations improve ( $\rho \approx 0.6$  to 0.7) when the lag between convective updraft/graupel volume and total LNO<sub>x</sub> production is accounted for.

7. The correlation between non-precipitation ice mass aloft and the average extent of all flashes is strong ( $\rho=0.82$ ), suggesting that the amount of anvil ice, which is likely carrying ample charge when the convective updraft is active, controls the average extent of flashes in ordinary multicell convection.

8. The average LNOM flash extent ramps up during the increase in the flash count. However, the average flash extent lags the flash count and both properties are somewhat anti-correlated (i.e., opposed). The largest average flash extents tend to occur after the maximum flash count associated with the convective generator.

9. Overall, the total flash extent of lightning flashes is largely controlled by total flash rate and not so much by average flash size. This result may be specific to ordinary multicell convection and more work is required to investigate this relationship in other storm types (e.g., supercells and mesoscale convective systems).

10. Cloud LNO<sub>x</sub> production is highly correlated to the total cloud flash extent ( $\rho=0.99$ ), which is strongly controlled by flash rate in this storm. Similarly, the correlation between ground LNO<sub>x</sub> production and ground flash extent is 0.95, although Koshak et al. [2014] note that other ground flash properties (e.g., peak current) can affect LNO<sub>x</sub> production.

11. Despite the fact that total cloud flash extent is much larger than total ground flash extent, the majority of LNO<sub>x</sub> production is still from ground flashes. In other words, LNOM produces significantly more LNO<sub>x</sub> on average for ground flashes (919 moles/flash) than for cloud flashes (116 moles/flash) in this multicell convection.

12. The LNO<sub>x</sub> production per ground flash is larger from 2026 to 2045 UTC when the average ground flash extent is larger. As noted earlier (see point 5), many of these extensive ground flashes are actually hybrid IC-CG flashes with large extents at heights above 6 km. This period accounts for some of the largest ground and hence total flash LNO<sub>x</sub> production for the storm. Since the ground flashes were small in number, the extent of individual ground flashes can have a significant impact on total LNO<sub>x</sub> production.

## ACKNOWLEDGMENTS

We wish to recognize funding from the National Science Foundation's Physical and Dynamical Meteorology (NSF PDM) Program (AGS-1063573), which has supported the DC3 field experiment and associated research. We also wish to thank the many, many people who made the collection of DC3 observations possible.

## REFERENCES

- Bain, A. L. 2013: Polarimetric Doppler radar and electrical observations of deep moist convection across northern Alabama during the Deep Convective Clouds and Chemistry Experiment. M.S. thesis, 148 pp., Dept. of Atmospheric Sciences, University of Alabama in Huntsville.
- Bain, A. L., R. Matthee, and L. D. Carey, 2013 : Polarimetric radar and electrical observations of deep moist convection across northern Alabama during the DC3 Experiment. Paper presented at *AMS 36th Conference on Radar Meteorology*, September 16-20, Breckenridge, CO, USA.
- Barth, M. C., W. Brune, C. Cantrell, S. A. Rutledge, J. H. Crawford, F. Flocke, H. Huntrieser, 2013: Overview of the Deep Convective Clouds and Chemistry Experiment, paper J7.1 presented at the *AMS 6<sup>th</sup> Conf. on the Meteorol. Appl. of Lightning Data*, January 5-10 2013, Austin, Texas.
- Barthe, C. and M. C. Barth, 2008: Evaluation of a new lightning-produced NO<sub>x</sub> parameterization for cloud resolving models and its associated uncertainties. *Atmos. Chem. Phys.*, **8**, 4691 – 4710.
- Barthe, C., W. Deierling, M. C. Barth, 2010: Estimation of total lightning from various storm parameters: A cloud-resolving model study. *J. Geophys. Res.*, **115**, D24202, doi:10.1029/2010JD014405.
- Bringi, V. N., V. Chandrasekar, 2001: Polarimetric Doppler Weather Radar Principles and Applications, Cambridge University Press, Cambridge, UK.
- Bringi, V. N., T. D. Keenan, V., Chandrasekar, 2001: Correcting C-Band radar reflectivity and differential reflectivity data for rain attenuation: A self-consistent method with constraints, *IEEE Trans. on Geo. and Rem. Sens.*, **39**, 1906-1915.
- Bruning, E. C. and D. R. MacGorman, 2013: Theory and observations of controls on lightning flash size spectra. *J. Atmos. Sci.*, **70**, 4012-4029.
- Carey, L. D. and S. A. Rutledge, 1996: A multiparameter radar case study of the microphysical and kinematic evolution of a lightning producing storm. *J. Meteorol. Atmos. Phys.*, **59**, 33–64.
- Carey, L. D. and S. A. Rutledge, 2000: The relationship between precipitation and lightning in tropical island convection: A C-Band polarimetric radar study. *Mon. Wea. Rev.*, **128**, 2687–2710.
- Carey, L.D., M.J. Murphy, T.L. McCormick and N.W.S. Demetriades, 2005: Lightning location relative to storm structure in a leading-line, trailing-stratiform mesoscale convective system. *J. Geophys. Res.*, **110**, D03105.
- Carey, L. D., A. L. Bain, and R. Matthee, 2014: Kinematic and microphysical control of lightning in multicell convection over Alabama during DC3. Paper presented at *5<sup>th</sup> International Lightning Meteorology Conference*, 20-21 March 2014, Tucson, Arizona, USA.
- Cooray, V., M. Rahman, and V. Rakov, 2009. On the NO<sub>x</sub> production by laboratory electrical discharges and lightning. *J. Sol. Atmos. Terr. Phys.*, **71**, 1877–1889.
- Cressman G. P., 1959: An operational objective analysis system. *Mon. Wea. Rev.*, **87**, 367-374.
- DeCaria, A.J., K.E. Pickering, G.L. Stenchikov, J.R. Scala, J.L. Stith, J.E. Dye, B.A. Ridley and P. Laroche, 2000 : A cloud-scale model study of lightning-generated NO<sub>x</sub> in an individual thunderstorm durin. STERAO-A, *J.*

*Geophys. Res.*, **105**, 11601 – 11616.

- DeCaria, A.J., K.E. Pickering, G.L. Stenchikov, and L.E. Ott, 2005 : Lightning-generated NO<sub>x</sub> and its impact on tropospheric ozone production : A three-dimensional modeling study of a Stratosphere-Troposphere Experiment : Radiation, Aerosols and Ozone (STERA0-A) thunderstorm. *J. Geophys. Res.* **110**, D14303.
- Deierling, W., and W. A. Petersen, 2008: Total lightning activity as an indicator of updraft characteristics. *J. Geophys. Res.*, **113**, D16210, doi:10.1029/2007JD009598.
- Deierling, W., W. A. Petersen, J. Latham, S. Ellis, and H. J. Christian, 2008: The relationship between lightning activity and ice fluxes in thunderstorms. *J. Geophys. Res.*, **113**, D15210, doi:10.1029/2007JD009700.
- Dye, J. E., J. J. Jones, W. P. Winn, T. A. Cerni, B. Gardiner, D. Lamb, R. L. Pitter, J. Hallett, and C. P. R. Saunders, 1986: Early electrification and precipitation development in a small, isolated Montana cumulonimbus. *J. Geophys. Res.*, **91**, 1231-1247.
- Dye, J. E., W. P. Winn, J. J. Jones, and D. W. Breed, 1989: The electrification of New Mexico thunderstorms. I. Relationship between precipitation development and the onset of electrification. *J. Geophys. Res.*, **94**, 8643-8656.
- Dye, J.E., and coauthors, 2000 : An overview of the Stratospheric-Tropospheric Experiment : Radiation, Aerosols, and Ozone (STERA0)-Deep Convection experiment with results for the July 10, 1996 storm. *J. Geophys. Res.*, **105**, 10023 – 10045.
- Fehr, T., H. Höller, and H. Huntrieser, 2004: Model study on production and transport of lightning-produced NO<sub>x</sub> in a EULINOX supercell storm. *J. Geophys. Res.*, **109**, D09102, doi:10.1029/2003JD003935.
- Goodman S. J., R. Blakeslee, H. Christian, W. Koshak, J. Bailey, J. Hall, E. McCaul, D. Buechler, C. Darden, J. Burks, T. Bradshaw, P. Gatlin, 2005: The North Alabama Lightning Mapping Array: Recent severe storm observations and future prospects. *Atmos. Res.*, **76**, 423-437.
- Heymsfield, A. J., and A. G. Palmer, 1986: Relations for deriving thunderstorm anvil mass of CCOPE storm water budget estimates, *J. Clim. Appl. Meteorol.*, **25(5)**, 691– 702.
- Koshak, W. J. and co-authors, 2004: North Alabama Lightning Mapping Array (LMA): VHF source retrieval algorithm and error analyses. *J. Atmos. Oceanic Technol.*, **21**, 543-558.
- Koshak, W., H. Peterson, A. Biazar, M. Khan and L. Wang, 2014: The NASA Lightning oxides model (LNOM): application to air quality modeling. *Atmos. Res.*, **135 – 136**, 363 – 369.
- Kuhlman, K. M., D. R. MacGorman, M. I. Biggerstaff, and P. R. Krehbiel, 2009: Lightning initiation in the anvils of two supercell storms. *Geophys. Res. Lett.*, **36**, L07802, doi:10.1029/2008GL036650.
- Loehrer, S. M., T. A. Edmands, and J. A. Moore, 1996: TOGA COARE Upper-Air Sounding Data Archive: Development and quality control procedures, *Bull. Amer. Meteor. Soc.*, **77**, 2651-2672.
- Matthee, R., and L. Carey, 2014: Storm physics and lightning properties over Northern Alabama during DC3. *XV International Conference on Atmospheric Electricity* (this conference), 15-20 June 2014, Norman, Oklahoma, USA.
- Miller, L. J. and T. Frederick, 1998: Custom Editing and Display of Reduced Information in Cartesian space, technical report published by the National Center for Atmospheric Research (NCAR), Mesoscale and Microscale Meteorology Division, June 1998, available at NCAR Earth Observation Laboratory's Radar Data Analysis Tools, <https://wiki.ucar.edu/display/raygridding/home>
- Mohr, C. G., L.J. Miller, R. L. Vaughn, and H. W. Frank, 1986: On the merger of mesoscale datasets into a common Cartesian format for efficient and systematic analysis, *J. Atmos. Oceanic. Technol.*, **3**, 143-161.

- Ott, L.E., K.E. Pickering, G. Stenchikov, H. Huntrieser, and U. Schumann, 2007 : Effects of lightning NO<sub>x</sub> production during the 21 July European Lightning Nitrogen Oxides Project storm studied with a three-dimensional cloud-scale chemical transport model. *J. Geophys. Res.*, **112**, D05307.
- Petersen, W. A., K. Knupp, J. Walters, W. Deierling, M. Gauthier, B. Dolan, J. P. Dice, D. Satterfield, C. Davis, R. Blakeslee, S. Goodman, S. Podgorny, J. Hall, M. Budge, A. Wooten, 2005: The UAH-NSSTC/WHNT ARMOR C-band Dual-Polarimetric Radar: A unique collaboration in research, education and technology transfer, paper presented at *AMS 32<sup>nd</sup> Radar Meteorology Conference*, Albuquerque, New Mexico.
- Peterson, H., Bailey, M., Hallett, J., Beasley, W., 2010. Reply to “Comment on ‘NO<sub>x</sub> production in laboratory discharges simulating blue jets and red sprites’ ”. *J. Geophys. Res.* **115**, A12306. <http://dx.doi.org/10.1029/2010JA015946>.
- Pickering, K.E., Y. Wang, W.K. Tao, C. Price, and J.-F. Müller, 1998: Vertical distributions of lightning NO<sub>x</sub> for use in regional and global chemical transport models. *J. Geophys. Res.*, **103**, 31203 – 31216.
- Price, C., J. Penner, and M. Prather, 1997 : NO<sub>x</sub> from lightning. 1. Global distribution based on lightning physics. *J. Geophys. Res.*, **102**, 5929 – 5941.
- Ridley, B. A., K. E. Pickering, and J. E. Dye, 2005: Comments on the parameterization of lightning-produced NO in global chemistry transport models. *Atmos. Environ.*, **39**, 6184–6187.
- Straka, J. M., D. S. Zrnić, R. V. Ryzhkov, 2000: Bulk hydrometeor classification and quantification using polarimetric radar data: Synthesis of relations, *J. Appl. Meteor.*, **39**, 1341–1372.
- Vivekanandan, J., D. S. Zrnić, S. Ellis, R. Oye, and A. V. Ryzhkov, 1999: Cloud microphysics retrievals using S-Band dual-polarization radar measurements, *Bull. Amer. Meteor. Soc.*, **80**, 381-388.
- Wang, Y., A.W. DeSilva, and G. C. Goldenbaum, 1998: Nitric oxide production by simulated lightning: Dependence on current, energy and pressure. *J. Geophys. Res.*, **103 (D15)**, 19149 – 19159.
- Weiss, S. A., D. R. MacGorman, and K. M. Calhoun, 2012: Lightning in the anvils of supercell thunderstorms. *Mon. Wea. Rev.*, **140**, 2064–2079.
- Wiens, K. C., S. A. Rutledge, and S. A., Tessorodorf, 2005: The 29 June 2000 supercell observed during STEPS. Part II: Lightning and charge structure. *J. Atmos. Sci.*, **62**, 4151-4177.
- Zipser, E. J. and K. R. Lutz, 1994: The vertical profile of radar reflectivity of convective cells: A strong indicator of storm intensity and lightning probability? *Mon. Wea. Rev.*, **122**, 1751-1759.